Gemmological Characterisation of Emeralds from Musakashi, Zambia, and Implications for Their Geographic Origin Determination

Michael S. Krzemnicki, Hao A. O. Wang, Markus Wälle, Pierre Lefèvre, Wei Zhou and Laurent E. Cartier

ABSTRACT: Emeralds from the Musakashi area of Zambia entered the gem trade in early 2002 in rather small quantities. Faceted stones are mostly available in smaller sizes (1–5 ct) but occasionally reach up to 20 ct or more. They can be of very fine gem quality and exhibit similarities to Colombian emeralds, not only in appearance, but also in their gemmological properties, inclusion features and chemical properties. Seventy-eight Musakashi emeralds were characterised gemmologically and chemically for this report. They can be distinguished from Colombian emeralds (as well as other similar emeralds from Afghanistan's Panjshir Valley) based on certain diagnostic internal features (e.g. 'sawtooth'-outlined multiphase fluid inclusions) and their chemical composition (e.g. plotting Fe vs V/Cr, and cluster visualisation using a t-SNE machine-learning algorithm). Separating them from the classic schist-hosted emeralds of the Kafubu area in Zambia is straightforward based on differences in their gemmological properties, inclusions, UV-Vis-NIR and Raman spectra, and chemical composition.

The Journal of Gemmology, **39**(4), 2024, pp. 338–350, https://doi.org/10.15506/JoG.2024.39.4.338

Emeralds from Zambia have been known for decades, mostly from mines along the Kafubu River in north-central Zambia (i.e. about 35 km south of the town of Kitwe). Kafubu-area emeralds have a schist-type origin (Zwaan *et al*. 2005; Giuliani *et al*. 2019) and account for the greatest share of Zambian emeralds in the gem trade. They are characterised by rather high Fe concentrations and inclusions such as mica, amphibole and feldspar, to name a few. In early 2002, emeralds from another Zambian source (Figure 1) were discovered at Musakashi in the Solwezi District (Zwaan *et al*. 2005), about 160 km west of Kitwe. However, this deposit has yielded only limited quantities, with about 15–20 kg of emeralds reported from the time of its discovery to late 2010 (Klemm 2010; Pardieu *et al*. 2015). Although some mining activity has continued intermittently in subsequent years, it has been limited due to legal issues surrounding the mining concessions (Klemm 2010; Pardieu *et al*. 2015; Karampelas & Pardieu 2024), which reportedly led locals to think the deposit was depleted. Interestingly, Musakashi emeralds are very different in their formation and occurrence from the classic schist-hosted Kafubu material.

Figure 1: Gem-quality emeralds investigated for this study from the Musakashi area of Zambia (here, 2.41–4.23 ct) resemble fine-quality emeralds from Colombia. Composite photo by Luc Phan, © SSEF.

According to Manyepa and Mutambo (2024), Musakashi emeralds are found 'in random pockets' related to weathered Cr-enriched metasediments that are cross-cut by hydrothermal veins (the source of Be necessary to crystallise emerald).

Musakashi emeralds are visually and chemically very similar to Colombian emeralds and to those from the Panjshir Valley in Afghanistan, thus presenting a challenge for geographic origin determination (Zwaan *et al*. 2005; Saeseaw *et al*. 2014).

PREVIOUS MUSAKASHI EMERALD DATA AND ERRATUM

Beginning in late 2017, faceted emeralds from Musakashi were submitted to the Swiss Gemmological Institute SSEF for testing without disclosure that they originated from this mining area in Zambia. Many of these stones were of exceptional quality but rather small (mostly 1–5 ct), and they were submitted either as single stones or in sets and parcels (e.g. Figure 2). Since then, we have analysed several hundred emeralds from this relatively new source in Zambia (even occasional larger stones up to 20 ct or more), although their quantity is far less than those circulating in the trade from Zambia's Kafubu mining area and from Colombia.

Several research samples reportedly from the Panjshir Valley were donated to SSEF a few years ago—from what at that time were considered reliable sources—but they were later found to be from Muskakashi. As a result, Krzemnicki *et al*. (2021a) erroneously described those samples as coming from recent production in Afghanistan. That article nevertheless provides a valuable contribution to the gemmological literature on emeralds, such as detailed inclusion photos and chemical data of emeralds from both the Panjshir Valley and the Laghman Province in Afghanistan. However, it is important for us to clarify that the data and inclusion features attributed to the so-called new emeralds from Afghanistan (referred to in that article as 'Panjshir type II') actually belong to those from Musakashi.

After the publication of the 2021 article, we received further research samples from Musakashi that were kindly provided by Dr Leo Klemm, who had visited the mining area in 2009 and 2010 (Klemm 2010). During that time he was able to acquire a few small specimens directly at the mining site. Thorough analysis of these and other documented Musakashi samples, as well as the occasional occurrence of similar stones in batches of small-sized Zambian emeralds submitted by clients, finally enabled us to uncover the mislabelling issue. We then reported the situation to the wider gemmological laboratory and gem trade community, which was not previously aware of such misrepresentation. These communications included a press release (SSEF 2021), a short note in *The Journal* (Krzemnicki *et al*. 2021b)

Figure 2: Examples of emeralds from Musakashi examined in the past few years at SSEF include a 21.22 ct pear shape (left) and a suite of cushion cuts ranging from 0.36 to 0.82 ct (total weight 14.6 carats). Composite photo by M. S. Krzemnicki, © SSEF.

and a brief publication in SSEF's *Facette Magazine* (Krzemnicki 2023).

The aim of the current article is to share a detailed and consolidated set of gemmological and chemical data on emeralds from Musakashi, with a focus on how to separate them from those of Colombia and Afghanistan, as well as other Zambian emeralds from Kafubu.

MATERIALS AND METHODS

For this study, we assembled a group of emeralds from Musakashi (78 samples, including 36 that were characterised by Krzemnicki *et al*. 2021a), Kafubu (105 samples), Colombia (92 samples, mainly from Muzo but also from Coscuez and Chivor) and Afghanistan's Panjshir Valley (hereafter referred to simply as Panjshir; 33 samples, including 11 from Krzemnicki *et al*. 2021a). Most of the emeralds were faceted, but there were a few rough samples with at least one polished surface. They were obtained mostly from the H. A. Hänni collection (SSEF research collection) and mining companies (e.g. Gemfields PLC and Muzo International SARL), but also from reputable gemmologists and emerald dealers. All of the samples were characterised by each of the techniques described below, except as otherwise noted.

Gemmological properties included the collection of RI and SG values, UV fluorescence reactions, and internal features as observed with a System Eickhorst Gemmaster microscope. Polarised ultraviolet-visible-near infrared (UV-Vis-NIR) absorption spectra were recorded for the o-ray using an Agilent Cary 5000 spectrometer (290–900 nm range, 0.35 nm step size and 0.5 s scan rate/step). For a few samples, we also used an in-house-developed portable unit equipped with an Avantes spectrometer (200–1000 nm range).

Fourier-transform infrared (FTIR) spectra were obtained with a Thermo Nicolet iS50 spectrometer (400–4000 cm^{-1} range and 4 cm^{-1} resolution) in diffuse reflectance mode, primarily to detect any fissure fillings (mainly oil) that may have been present in some of the samples.

Raman analyses of selected emeralds and their inclusions were performed with a Renishaw inVia spectrometer (1.5 cm^{-1} spectral resolution) coupled with a Leica DM2500 M microscope and an argon-ion laser (514.5 nm excitation). All analyses were carried out in confocal mode using the 20× objective of the microscope to focus on the emerald surface or on inclusions. For the analysis of water molecule orientation in the emeralds, the *c*-axis was oriented perpendicular to the electric field vector of the laser beam (i.e. E⊥c; cf. Huong *et al*. 2010).

Chemical analysis of the emeralds was carried out by energy-dispersive X-ray fluorescence (EDXRF) spectroscopy and by laser ablation inductively coupled plasma time-of-flight mass spectrometry (LA-ICP-TOF-MS). EDXRF data were collected using a Thermo Scientific ARL Quant'X spectrometer in vacuum mode. LA-ICP-TOF-MS analyses were done using SSEF's GemTOF platform, consisting of a 193 nm ArF excimer laser equipped with a TwoVol2 ablation chamber (NWR193UC from Elemental Scientific Lasers) and coupled with a commercial ICP-TOF-MS unit (*icp*TOF from Tofwerk AG) that was modified from an optimised ICP-Q-MS unit (iCAP Q from Thermo Fisher Scientific). On each sample we analysed three or four spots (100 µm diameter) on visually inclusion-free areas. All spots were ablated at 20 Hz and with a fluence of 5.6 J/cm^2. Helium was used as the carrier gas (0.8–0.9 L/min). Five pre-cleaning laser shots were fired at the beginning of each measurement (30 s ablation time). We used NIST SRM 610 and SRM 612 glasses as external standards, and $^{29}Si^+$ (for ideal beryl) as an internal standard. Further details about instrumental parameters, analytical conditions, data processing and plotting can be found in Wang *et al*. (2016) and Wang and Krzemnicki (2021).

The GemTOF data were analysed using t-distributed stochastic neighbour embedding (t-SNE), a machine-learning algorithm for the non-linear transformation of high-dimensional data sets (such as multi-element concentrations from mass spectrometry) into a low-dimensional space (van der Maaten & Hinton 2008). The unsupervised algorithm used by this technique means that the data input into the statistical calculation were not labelled with their origin *a priori*. The t-SNE scatter points are colour-coded according to their respective origins only after t-SNE analysis, and the clustering or grouping of data points is purely due to their elemental similarities. This method allows us to better visualise sample relationships and place separate data sets into various subgroups. A detailed description of this statistical methodology for an emerald case study is provided in Wang and Krzemnicki (2021). In the present study, we calculated t-SNE plots using concentrations of 56 elements from 1,088 spot analyses of 308 total emerald samples.

RESULTS AND DISCUSSION

Table I presents a summary of the gemmological properties of the Musakashi emeralds compared with samples from Kafubu, Colombia and Panjshir. The data show similarities between the Musakashi and Colombian emeralds in terms of their physical properties (e.g. RI and SG), whereas the Fe-enriched schist-type emeralds from Kafubu are easily distinguishable by their higher RI and SG values.

Internal Features

The most common and striking internal features in Musakashi emeralds were bundles of hollow channels oriented parallel to the *c*-axis (Figure 3). Although not present in all samples, these channels were generally much more visible than the similar but finer tubes parallel to the *c*-axis that often occur in Colombian emeralds (Bosshart 1991).

In addition, many of the studied Musakashi emeralds contained irregularly curved (Figure 4a) to kinked (Figure 4b) hollow tubes (possibly etch channels), some of which emerged in comet-like fashion from a colourless inclusion (feldspar, identified by Raman spectroscopy; Figure 4c). Cavities and channels were partly filled with orange Fe-hydroxide (Figures 4d–f), a feature very unlikely to be found in Colombian emeralds based on the authors' experience. In general, Musakashi emeralds are very homogeneous and exhibit a beautifully saturated green colour, although fine, subtle growth lines were present occasionally (Figure 4g), sometimes combined with swirl- or chevron-like features (Figures 4h–i).

Table I: Gemmological properties of emeralds from Zambia (Musakashi and Kafubu), Colombia and Afghanistan's Panjshir Valley.

Locality	Zambia (Musakashi)	Zambia (Kafubu)	Colombia	Afghanistan (Panjshir Valley)
No. samples	78	105	92	33
Weight range	0.11–21.22 ct	0.64–31.56 ct	0.34–64.35 ct	0.62–13.79 ct
RI	1.576–1.586	1.580–1.592	1.568–1.582	1.581–1.589
Birefringence	0.006–0.009	0.007–0.010	0.006–0.008	0.006–0.009
SG	2.72–2.76	2.74–2.80	2.70–2.75	2.73–2.76
Long-wave UV reaction*	None to moderate red	None	None to distinct red	None to weak red
Internal features				
Colour zoning	Uncommon; homogeneous colour	Occasional; homogeneous to distinct colour zoning	Common; often distinct colour zones perpendicular to *c*-axis	Uncommon; occasional hexagonal colour zoning
Growth structures	Fine, subtle growth lines parallel to *c*-axis, partly swirl- to chevron-like	Occasional growth lines parallel to prism faces and basal pinacoid	Occasional growth lines perpendicular to *c*-axis, partly strong graining	Dense growth lines parallel to *c*-axis
Hollow channels	Fine and often densely arranged parallel to *c*-axis, partly kinked or slightly curved	Occasional fine and short hollow tubes parallel to *c*-axis	Very fine and often densely arranged parallel to *c*-axis	Coarse to fine, parallel to *c*-axis, often filled with brown Fe-hydroxide
Fe-hydroxide	Occasional flat, semi-circular cavities partially filled with Fe-hydroxide	Occasional	Rare	Common
Fluid inclusions	Small, spiky to irregular and 'sawtooth' multiphase	Commonly rectangular two- and three-phase; isolated two-phase negative crystals	Spiky three-phase; few multiphase	Spiky multiphase, often stretched along *c*-axis
Solid inclusions	Few: feldspar, apatite and rutile	Frequent: actinolite-tremolite, phlogopite, apatite, magnetite, quartz and whitish decrepitated disc-like inclusions	Occasional: calcite, pyrite, quartz and apatite	Occasional: pyrite, dolomite, rutile and feldspar

* All samples were inert to short-wave UV radiation.

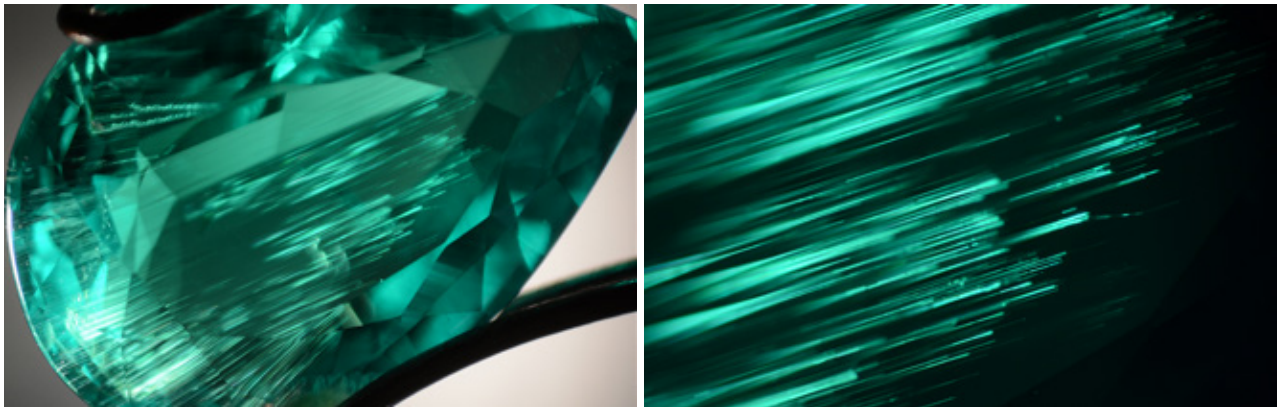

Figure 3: Noticeable hollow channels oriented parallel to the *c*-axis are one of the most common and distinctive internal features in the Musakashi emeralds. Photomicrographs by M. S. Krzemnicki, © SSEF; magnified 10× (left) and 50× (right).

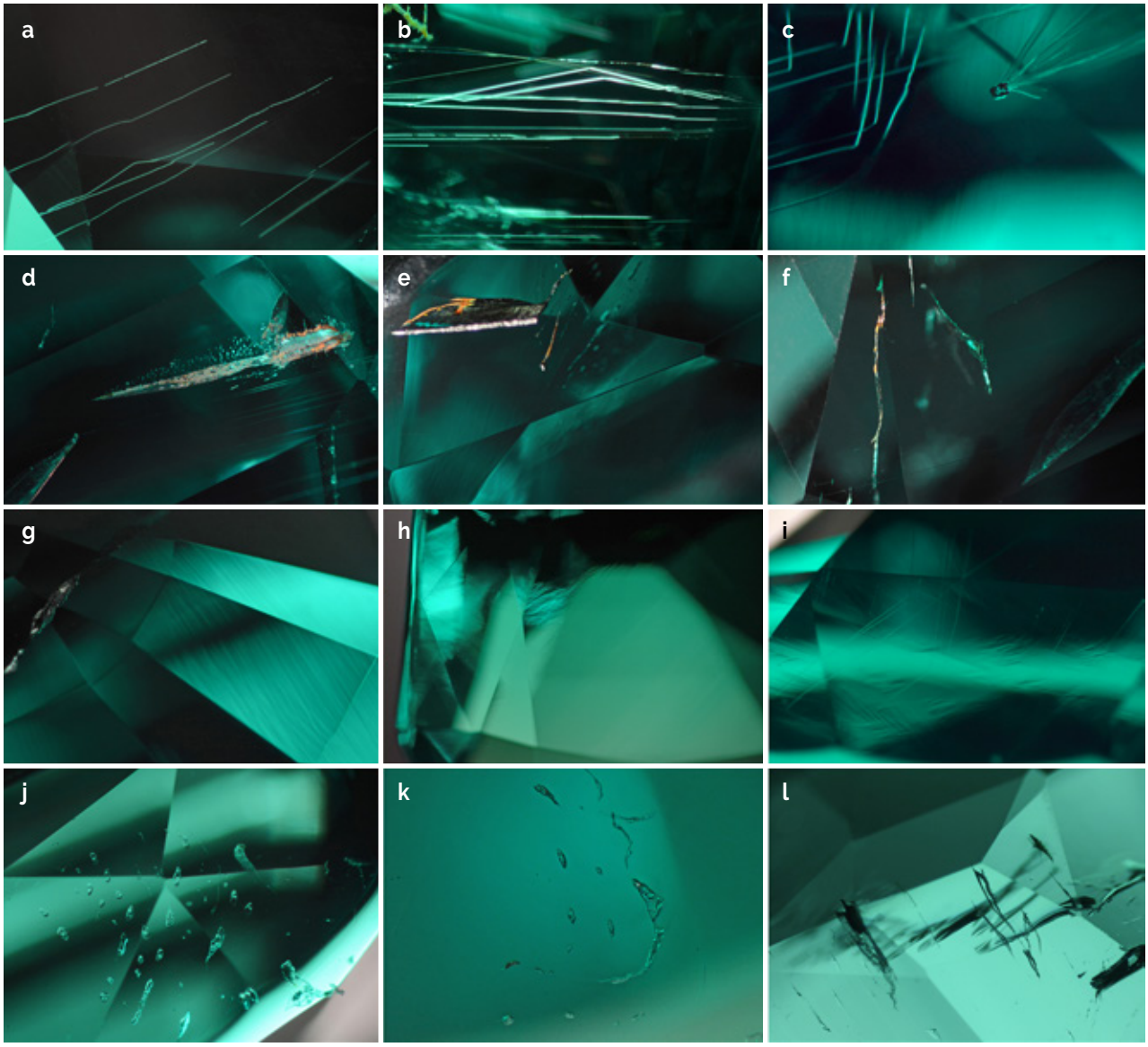

Figure 4: Characteristic inclusions in the Musakashi emeralds include: (**a**, **b**) curved to kinked channel structures; (**c**) a comet-like assemblage consisting of channels emerging from a feldspar grain; (**d–f**): orange Fe-hydroxide in hollow channels and flat semi-circular cavities; (**g–i**) fine growth lines and chevron-like growth structures; and (**j–l**) spiky to irregular and sawtooth-edged multiphase fluid inclusions. Photomicrographs by M. S. Krzemnicki, © SSEF; magnified 30× (j and l), 50× (a–c, e–i and k) and 60× (d).

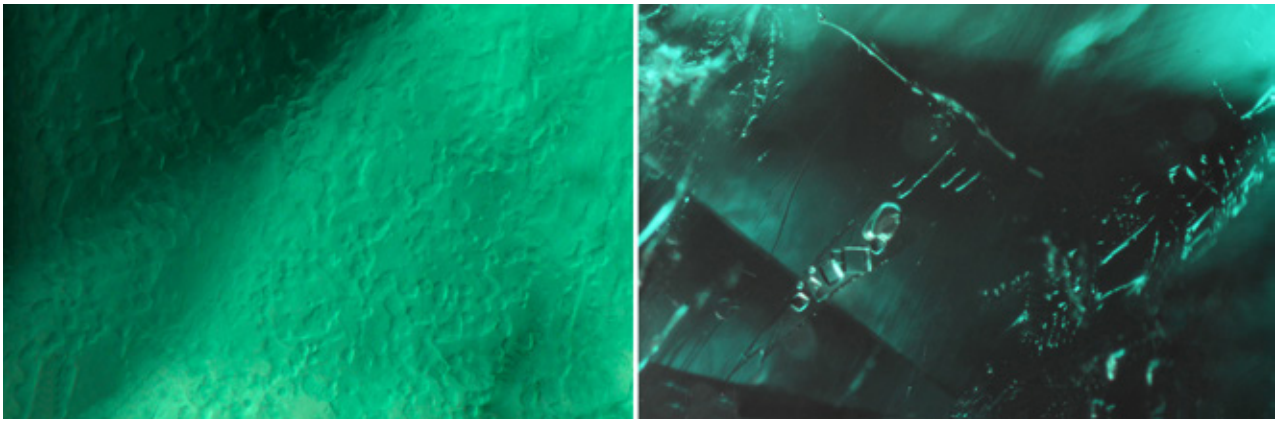

Figure 5: (**a**) *Gota de aceite* graining is characteristic of Colombian emeralds. (**b**) The multiphase inclusions seen here in an emerald from Colombia resemble those observed in our samples from Musakashi (see, e.g., Figures 4j and 4k). Photomicrographs by M. S. Krzemnicki, © SSEF; magnified 50×.

We did not encounter the honeycomb graining effect (*gota de aceite*; Figure 5a) well known from Colombian emeralds in any of the Musakashi samples investigated for this study. Fluid inclusions occurred in the Musakashi emeralds as spiky to irregular multiphase inclusions (Figures 4j–k). However, it is not possible to separate emeralds from Musakashi and Colombia based on fluid inclusions (multiphase vs 'classic' Colombian three-phase jagged-shaped fluid inclusions consisting of a salt solution, a gas bubble and a salt crystal), because we occasionally observed similar multiphase inclusions that contained several solid salt crystals in Colombian emeralds (see Figure 5b).

Interestingly, some of the multiphase fluid inclusions in our Musakashi samples showed a distinct 'sawtooth' outline (Figures 4l and 6), which in our opinion is highly characteristic for emeralds from this locality.

By contrast, the emerald samples from Kafubu showed very different inclusion features. They were mainly characterised by rectangular two- and three-phase fluid inclusions oriented parallel to the *c*-axis, commonly with isolated two-phase negative crystals. Also present were randomly oriented phlogopite and colourless prismatic to slightly curved needle-like amphibole. For a detailed description of inclusions in Kafubu emeralds, see Zwaan *et al*. (2005).

The characteristic internal features in Panjshir emeralds included spiky-to-tubular multiphase fluid inclusions containing halite-sylvite, a few solid inclusions such as pyrite, dolomite, rutile and feldspar (all identified by Raman spectroscopy), as well as fine to rather coarse hollow tubes oriented parallel to the *c*-axis (see also the 'Panjshir type I' emeralds in Krzemnicki *et al*. 2021a).

UV-Vis-NIR Spectra

Representative absorption spectra for our samples from Musakashi, Kafubu, Colombia and Panjshir are shown in Figure 7. They are all similarly characterised by two Cr^{3+} (and/or V^{3+})-related absorption bands in the visible range, but differ mainly in the intensity (from absent to strong) of the broad Fe^{2+}-related absorption band in the near-infrared region. The green colour of emerald is not solely due to the presence of Cr, but to a complex interplay of the transition metals Cr, V and Fe in the beryl structure. In the polarised UV-Vis-NIR spectrum (ordinary ray, equivalent to E⊥c) of emerald, the octahedrally coordinated Cr^{3+} and/or V^{3+} chromophores produce two broad absorption bands at about 435 and 605 nm, as well as small, sharp, spin-forbidden Cr bands in the 600–700 nm range (Wood & Nassau 1968; Schmetzer 2014 and references therein).

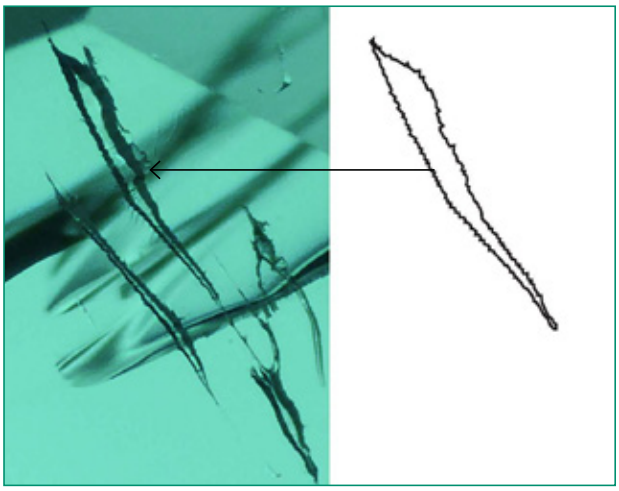

Figure 6: Tubular fluid inclusions with a distinctive sawtooth outline (expanded here from Figure 4l) are characteristic of Musakashi emeralds, and can be used to distinguish them from emeralds of similar appearance from other localities. Photomicrograph by M. S. Krzemnicki, © SSEF; magnified 70×.

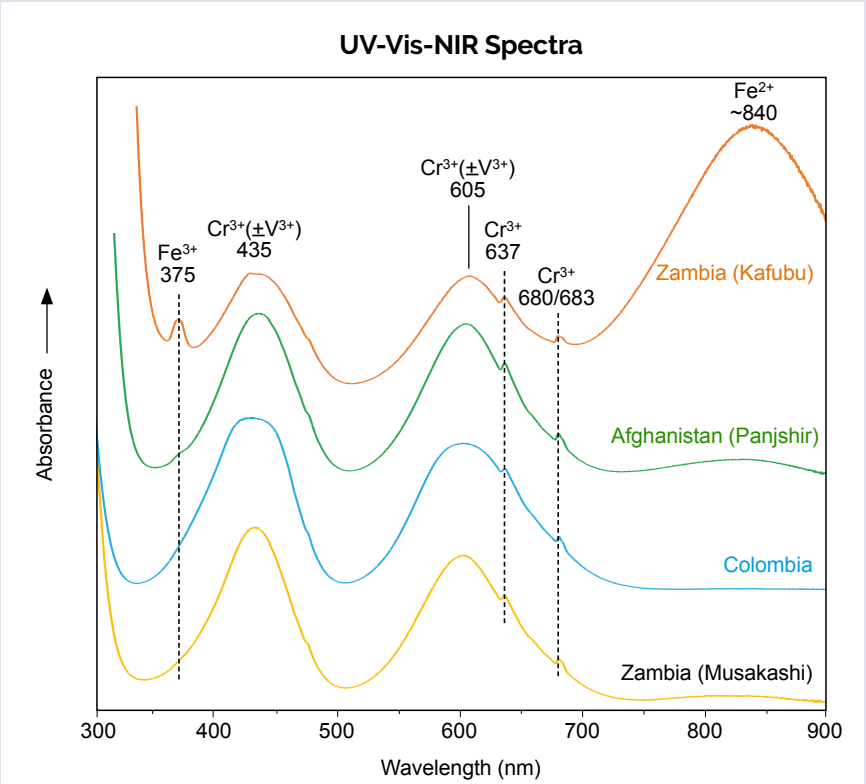

Figure 7: Polarised UV-Vis-NIR absorption spectra (o-ray) of representative emerald samples show similarities between those from Musakashi and Colombia. The spectrum of the Kafubu emerald is clearly different, with a distinct Fe^{2+}-related band in the near-infrared region, although the same Fe^{2+}-related band is present but very weak in the Musakashi emerald spectrum. The spectrum of the Panjshir emerald is rather similar to that of Musakashi, but with a more pronounced Fe^{2+}-related band in the near infrared. The spectra are offset vertically for clarity.

The presence of octahedrally coordinated Fe^{2+} in beryl (and emerald) results in a broad absorption band at about 840 nm in the near-infrared region (Wood & Nassau 1968; Taran & Rossman 2001). The Musakashi emeralds commonly exhibited a weak Fe^{2+}-related band in this region. Although mostly absent from Colombian emeralds, a similar weak feature was also found in the relatively Fe-rich Colombian emeralds investigated for this study, thus making a separation of emeralds from these two sources unreliable based on this criterion. In the Panjshir emeralds, this Fe^{2+}-related band in the near-infrared was more pronounced compared to the Musakashi and Colombian emeralds. As seen in Figure 7, the Fe-rich schist-type emeralds from Kafubu could be easily distinguished from the Musakashi and Colombian stones by their distinct-to-strong Fe^{2+}-related absorption band in the near infrared.

Raman Spectroscopy: Type I and Type II H_2O

Beryl readily accommodates water molecules into its channel structures parallel to the *c*-axis (Wood & Nassau 1968; Huong *et al*. 2010; Groat *et al*. 2014). The orientation of these channel H_2O molecules depends mainly on the presence (and amount) of alkali-metal elements (Li, Na, K, Rb and Cs) in the channels. The H_2O molecule orientation can be detected by FTIR (Wood & Nassau 1968) or Raman spectroscopy. We used the latter to investigate the average orientation of H_2O molecules in our emerald samples based on the relative intensity of the Raman bands at 3608 cm^{-1} (type I H_2O) and 3598 cm^{-1} (type II H_2O; Huong *et al*. 2010).

The Raman spectra for the Musakashi and Colombian emeralds were similar, with a dominant type I H_2O band at 3608 cm^{-1} (Figure 8). This indicates that the axis of the H_2O molecules is predominately perpendicular to the beryl *c*-axis (and channel axis; see Wood & Nassau 1968; Huong *et al*. 2010). This is also consistent with their low concentrations of alkali-metal elements (see below). By contrast, the Kafubu emeralds revealed a dominant Raman band at 3598 cm^{-1} (type II H_2O), indicating that the H_2O molecules are oriented with their axis parallel to the beryl *c*-axis, which is characteristic of emeralds hosted in mafic to ultramafic host rocks (i.e. deposit types IA and IIA; Giuliani *et al*. 2019). They typically contain notable amounts of alkali metals in the channels of the beryl structure, thus affecting the orientation of the H_2O molecules. Emeralds from Panjshir generally show relatively equal intensities of the two H_2O bands, thus indicating no particular abundance of either of the water molecule orientations (see figure 8 in Krzemnicki *et al.* 2021a).

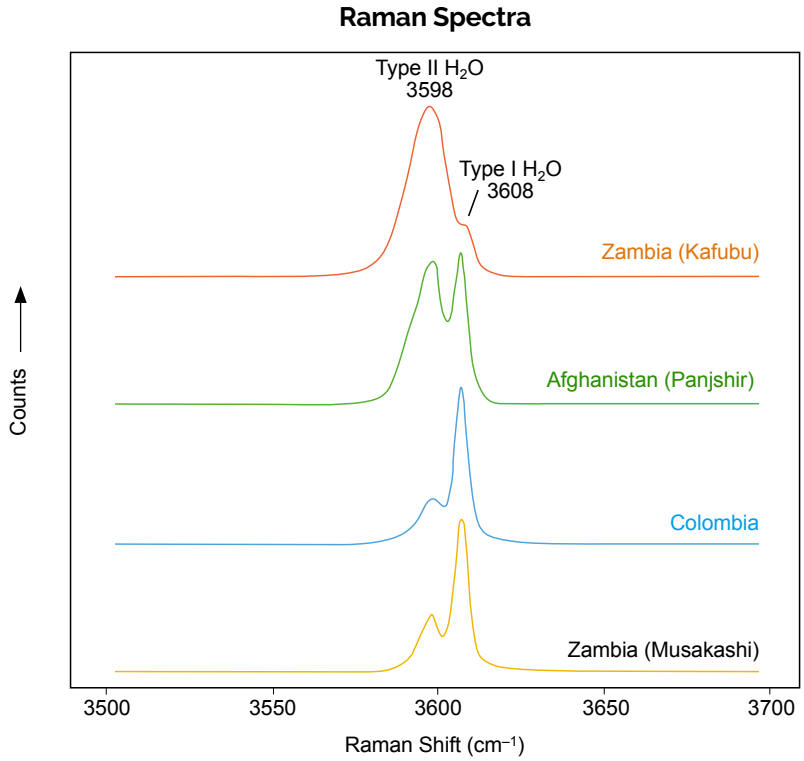

Figure 8: Raman spectra in the 3500–3700 cm^{-1} region illustrate various intensities of the bands corresponding to the two orientations of channel H_2O molecules—type I and type II H_2O (Huong *et al.* 2010)—for emeralds from the four origins. The spectra are offset vertically for clarity.

Thus, comparing the water-molecule bands in Raman (or FTIR) spectra can distinguish, at least in part, the geographic origins of emeralds, by differentiating those of Kafubu and Panjshir from those of Musakashi and Colombia.

Chemical Analyses and Machine-learning Data Visualisation

Table II provides a summary of the minor- and trace-element data obtained by LA-ICP-TOF-MS for the Musakashi emeralds as compared to those from Kafubu, Colombia and Panjshir. A more extensive table containing the complete data set is accessible in *The Journal*'s online data depository. EDXRF data are not included here, but showed the same trends and correlations as the LA-ICP-TOF-MS data for the elements that could be analysed by EDXRF spectroscopy.

Chemical Trends. Our analyses revealed distinct chemical differences between the Musakashi and Kafubu emeralds, consistent with their very different geological settings: hydrothermal veins at Musakashi and schist associated with altered metabasite at Kafubu (Zwaan *et al*. 2005 and references therein). This geological difference is evident when comparing the average concentrations of Fe (8,580 ppm for Kafubu vs 1,490 ppm for Musakashi), and also the sum of the alkali and alkaline-earth elements (Li, Na, Mg, K, Ca, Rb and Cs), which was high in the emeralds from Kafubu (about 30,000 ppm) compared to those from Musakashi (about 9,000 ppm). By contrast, the chemical data for Musakashi and Colombian emeralds were very similar, as were their visual, gemmological and inclusion features (see Table I). Specifically, the Musakashi and Colombian emeralds contained relatively low Na, Mg and Fe, and distinctly higher V, compared to those from Kafubu. Panjshir emeralds were chemically more similar to those from Kafubu, except that they generally contained more V and less Fe.

Chemical differences in the emeralds from Kafubu vs Colombia and Musakashi were also evident from other trace elements, such as Rb and Cs, in addition to the transition elements Mn, Co and Ni, which are commonly enriched in metabasites and thus were found at higher concentrations in the Kafubu emeralds. Our Panjshir emeralds had similar Rb concentrations as the Kafubu emeralds, but contained low amounts of the transition elements Mn, Co and Ni. Interestingly, the Panjshir emeralds also commonly contained distinct traces of Sc (average value of 818 ppm), although they showed a large overlap with Colombian emeralds and to a

Table II: Summary of LA-ICP-TOF-MS data of emeralds from Zambia (Musakashi and Kafubu), Colombia and Afghanistan's Panjshir Valley.*

Locality	Zambia (Musakashi)	Zambia (Kafubu)	Colombia	Afghanistan (Panjshir Valley)
No. samples (no. analyses)	78 (273)	105 (393)	92 (306)	33 (116)
Element (ppm)				
Li	65.3–109 (89.5)	271–1380 (648)	22.2–146 (48.0)	65.3–218 (117)
Na	2870–6440 (4520)	7990–17400 (13600)	688–8770 (5610)	6730–14400 (10100)
Mg	2570–6680 (4110)	4990–46000 (13000)	605–8430 (5480)	5864–15719 (10300)
K	22.5–143 (44.3)	141–17400 (489)	bdl–73.4 (<38.0)	181–1600 (728)
Ca	bdl–1080 (<538)	bdl–1120 (<721)	bdl–613 (<350)	236–941 (495)
Sc	36.8–840 (179)	22.0–304 (85.0)	8.66–1490 (149)	71.1–2780 (818)
V	537–3680 (1380)	30.9–472 (120)	303–9780 (2940)	242–6280 (1410)
Cr	1630–9610 (3480)	509–10620 (2460)	50.8–6990 (2290)	240–5390 (2310)
Mn	0.30–1.01 (0.59)	6.06–156 (31.2)	0.04–3.01 (0.37)	0.72–4.40 (1.99)
Fe	1070–2260 (1490)	4460–18400 (8580)	101–1940 (536)	1010–11300 (4280)
Co	bdl–0.13 (<0.04)	1.44–15.1 (2.90)	bdl–0.04 (<0.02)	bdl–0.21 (<0.10)
Ni	0.50–9.10 (1.73)	4.46–229 (19.8)	bdl–2.17 (<0.58)	bdl–9.88 (<1.54)
Zn	0.33–16.3 (0.84)	5.41–208 (41.4)	bdl–1.34 (<0.22)	bdl–1.34 (<0.43)
Ga	13.9–36.2 (21.2)	6.25–22.3 (13.8)	8.18–64.9 (26.9)	10.9–43.0 (23.9)
Rb	1.70–4.75 (3.09)	17.4–382 (60.4)	0.20–5.81 (3.30)	15.4–104 (50.7)
Cs	5.48–11.7 (8.39)	221–3860 (1140)	3.35–21.2 (12.5)	23.2–79.5 (43.2)

* Data include element ranges with average values in parentheses. Musakashi samples include 44 emeralds from Krzemnicki *et al.* (2021a) that were mislabelled 'Panjshir type II'. Abbreviation: bdl = below detection limit.

lesser extent with those from Musakashi and Kafubu (see Table II).

Geographic Origin Determination. Attributing a geographic origin to emerald based on chemical data is well known in the gemmological literature. Distinctions are mainly based on significant elemental substitutions that can occur on different lattice sites in the beryl structure when emeralds form in different geological settings (Cronin & Rendle 2012; Schwarz & Klemm 2012; Groat *et al*. 2014; Schwarz 2015; Aurisicchio *et al*. 2018; Giuliani *et al*. 2019; Karampelas *et al*. 2019; Schwarz & Curti 2020).

A bivariate plot of our data for Rb vs Cs (Figure 9) reveals that emeralds from Kafubu and Panjshir are distinct from Musakashi and Colombian emeralds, whereas the data clusters of the latter two overlap considerably, which further demonstrates their trace-element similarity. A plot of Fe vs V (Figure 10a) also shows that distinguishing between Musakashi and Colombian emeralds remains ambiguous due to overlapping data points, whereas Kafubu emeralds again are clearly separated. However, by plotting Fe vs V/Cr, emeralds from Musakashi and Colombia are separated (Figure 10b).

Distinctions also can be achieved by applying an automated statistical algorithm (such as t-SNE) for the purposes of data reduction and visualising of how complex multi-dimensional data sets cluster (e.g. trace elements). Artificial intelligence—especially machine-learning algorithms—has recently become an important tool in gemmological research (Bindereif *et al*. 2020; Wang & Krzemnicki 2021; Alonso-Perez *et al*. 2024; Bendinelli *et al*. 2024), notably for origin determination. The authors have applied such machine-learning algorithms for many years, specifically for the origin determination of emerald and Paraíba-type tourmaline, amongst other gems (Wang *et al*. 2019, 2021). For a detailed description of the unsupervised t-SNE algorithm and its use in gemmology, see Wang and Krzemnicki (2021).

The t-SNE plot in Figure 11 (based on 56 analysed elements) shows how effectively this machine-learning approach can separate Zambian emeralds (i.e. Musakashi and Kafubu) from Colombian and Afghan emeralds, despite the fact that emeralds from Musakashi and Colombia have similar chemical

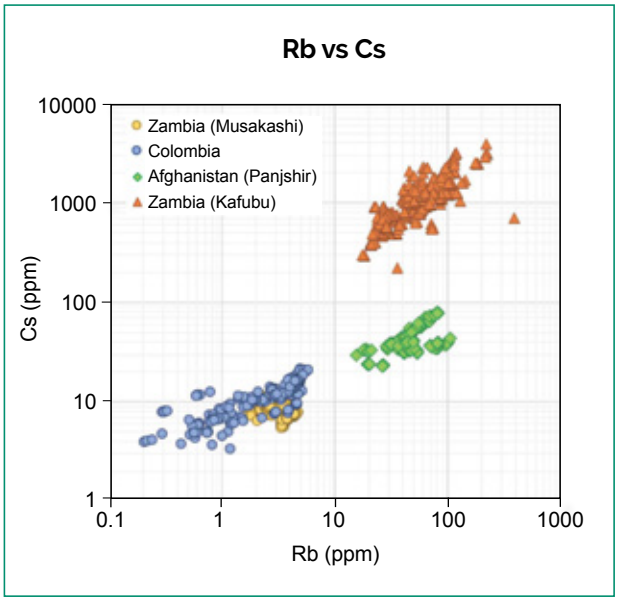

Figure 9: A plot of Rb vs Cs for the analysed emeralds from Musakashi, Kafubu, Panjshir and Colombia shows distinct clusters for Kafubu and Panjshir, with a third cluster in which Musakashi and Colombian emeralds overlap.

properties and often display overlapping data points in bivariate scatter plots (e.g. Figures 9 and 10a). Data clusters corresponding to each locality show excellent separation; a rotational video clip of Figure 11 is also available in *The Journal*'s online data depository.

Elemental differences between the Musakashi and Colombian emerald data clusters can be visualised in greater detail in the series of diagrams shown in Figure 12, in which the relative concentrations of selected trace elements have been superposed on two-dimensional t-SNE plots. The diagrams provide a qualitative indication of which elements are causing the separation of the Musakashi and Colombia data clusters, and show that most of the Colombian emeralds contain distinctly lower Li, Fe and Zn, and higher Cs, than the Musakashi emeralds. Interestingly, the V concentrations in emeralds from both origins cover a rather large and similar range, but with some Colombian emeralds having distinctly greater V (dark red spots in that diagram) than Musakashi emeralds (spots only ranging up to orange). This is confirmed by the data presented in Table II.

CONCLUSIONS

Emeralds from Musakashi in the Solwezi District of north-central Zambia were first discovered in early 2002, but initially only a very limited quantity of stones found their way into the gem trade. This study presents for the first time a detailed characterisation of emeralds from Musakashi, many of which are of very fine gem quality resembling the best Colombian emeralds. Musakashi emeralds differ in many aspects (geological setting, properties, chemical composition and even visual appearance) from those of the much larger deposits along the Kafubu River in Zambia, which have produced by

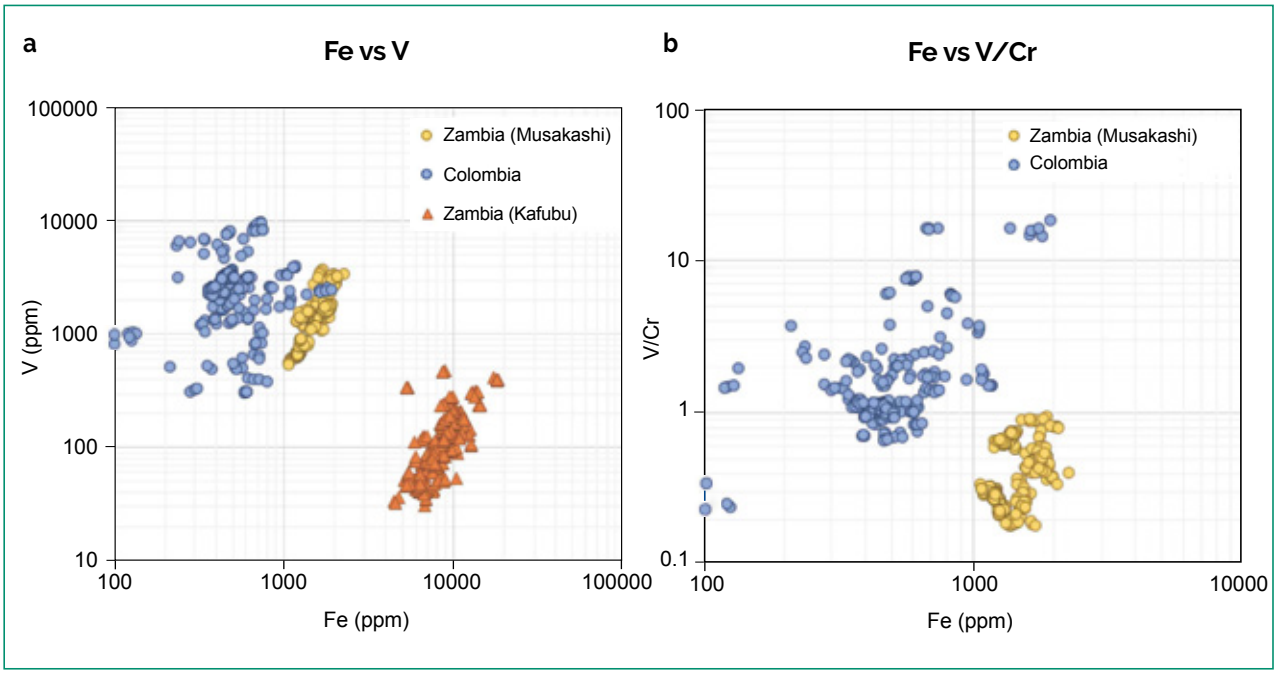

Figure 10: (**a**) In a plot of Fe vs V, Kafubu emeralds are distinctly separate from Musakashi (and Colombian) emeralds. (**b**) By plotting Fe vs V/Cr, emeralds from Musakashi and Colombia can be separated into two distinct populations.

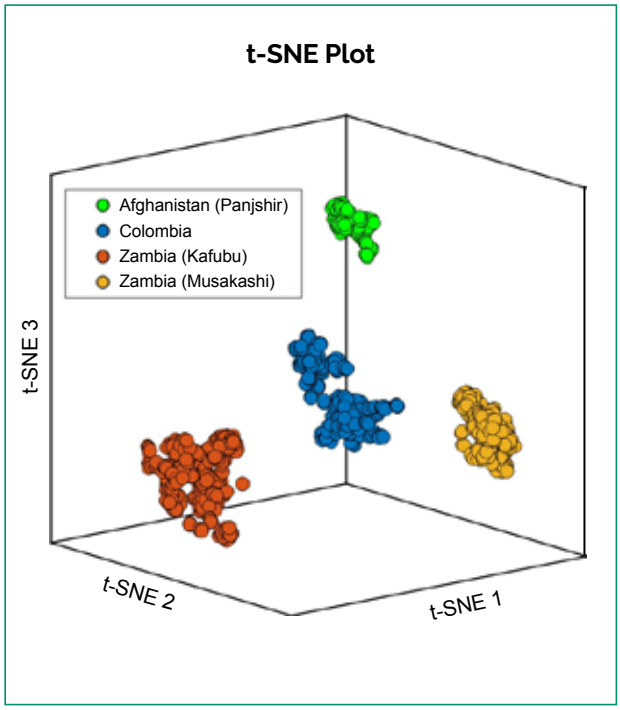

Figure 11: A three-dimensional t-SNE scatter plot shows well-defined clustering of emeralds based on their origin. The Zambian emeralds from Musakashi and Kafubu form distinct clusters, which are clearly separated from the clusters representing emeralds from Colombia and Panjshir. The axes in this t-SNE plot do not correspond to specific sets of elements but rather provide a visual representation of the similarity patterns among the 56 elements analysed in this study.

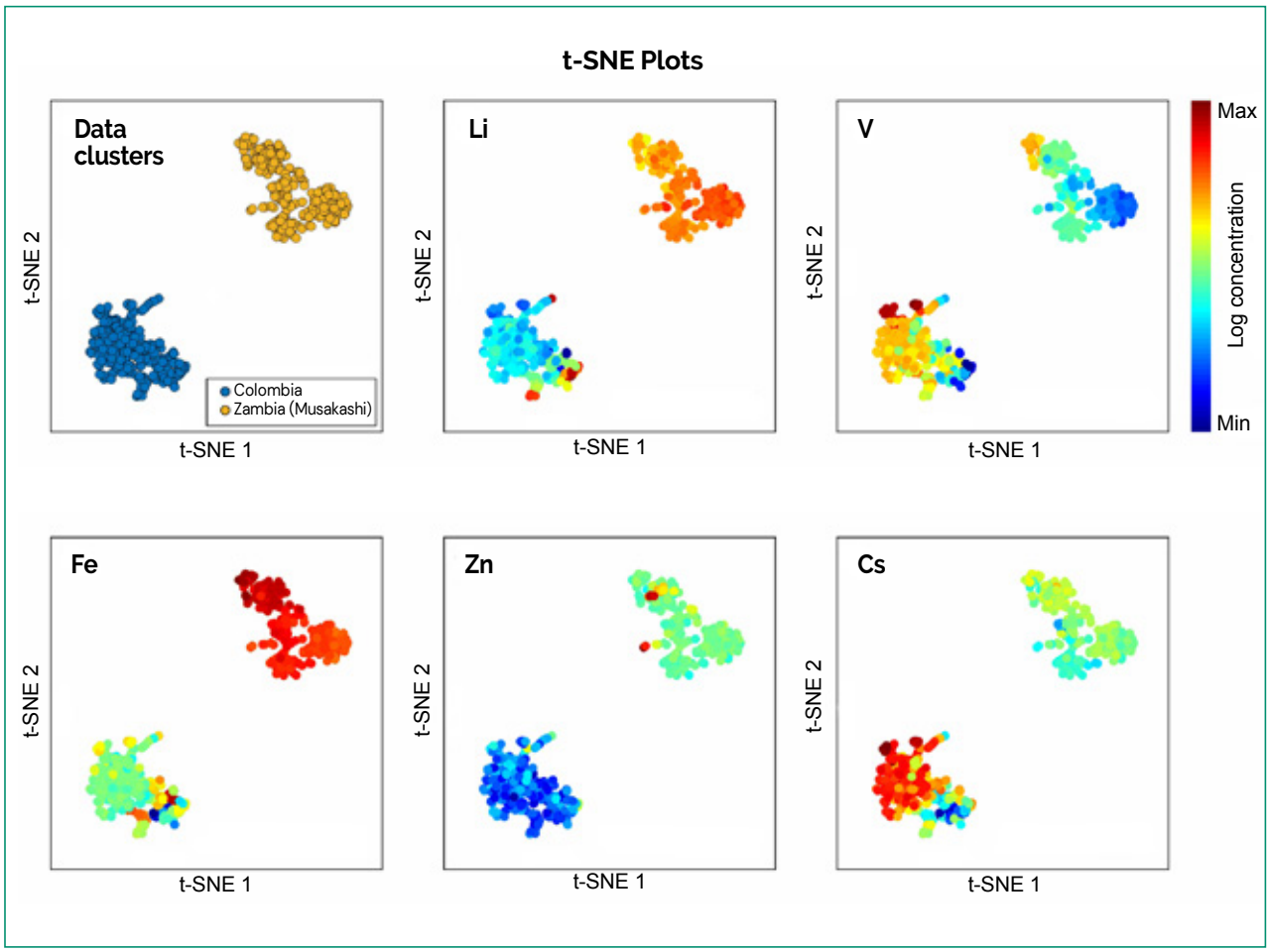

Figure 12: Two-dimensional t-SNE scatter plots comparing Musakashi and Colombian emeralds are combined with selected trace-element concentrations. The plots highlight the elemental differences between the two clusters. The colour scale represents the minimum to maximum concentrations of the respective elements on a logarithmic scale, further enhancing the distinction between the emeralds from these two localities.

far the greatest quantity of Zambian emeralds in the gem trade to date.

One aim of this article is to correct a previous publication about Afghanistan emeralds (Krzemnicki *et al*. 2021a), in which Musakashi emeralds were inadvertently mislabelled as 'Panjshir type II' material on the basis of erroneous locality information provided for the samples. In addition, a special focus of this study is the comparison between emeralds from Musakashi and those of similar appearance from Colombia as well as from Afghanistan's Panjshir Valley. The inclusion features in Musakashi emeralds are very different from those of Kafubu (e.g. jagged multiphase inclusions vs rectangular two- and three-phase inclusions in the latter), but may closely resemble those of Colombian emeralds. Similarly, UV-Vis-NIR spectra can reliably distinguish Musakashi from Kafubu emeralds (mainly based on the Fe^{2+}-related band in the near-infrared region), but their spectra largely overlap with those of Colombian (and to a lesser extent Panjshir) emeralds. Another option to distinguish Musakashi emeralds from those of Kafubu and Panjshir is based on the orientation of channel H_2O molecules analysed by FTIR or Raman spectroscopy, but this approach does not allow a distinction between Musakashi and Colombian emeralds.

Using chemical analyses, it is possible to unambiguously distinguish emeralds from these selected four geographic origins based on elemental scatter plots and machine-learning algorithms for data visualisation. A plot of Rb vs Cs provides a clear separation of the emeralds into three groups: those from Kafubu, those from Panjshir and a closely overlapping group from Musakashi and Colombia. In addition, plotting Fe vs V separates Kafubu emeralds from those of Musakashi and Colombia, and Fe vs V/Cr additionally separates Musakashi and Colombian emeralds. Geographic origin determination is further supported by using a machine-learning approach (unsupervised t-SNE algorithm), which offers an even more pronounced demonstration of the chemical distinction of Musakashi emeralds from those of Kafubu, Colombia and Panjshir.

Although all the chemical data presented in this study were acquired by LA-ICP-TOF-MS (GemTOF), it is important to note that the bivariate scatter plots in Figure 10 (Fe vs V and Fe vs V/Cr) are useful even for gemmological laboratories which only have access to EDXRF spectroscopy, as the same trends and correlations were found in the EDXRF analyses of our samples.

REFERENCES

Alonso-Perez, R., Day, J.M.D., Pearson, D.G., Luo, Y., Palacios, M.A., Sudhakar, R. & Palke, A. 2024. Exploring emerald global geochemical provenance through fingerprinting and machine learning methods. *Artificial Intelligence in Geosciences*, **5**, article 100085, https://doi.org/10.1016/j.aiig.2024.100085.

Aurisicchio, C., Conte, A.M., Medeghini, L., Ottolini, L. & De Vito, C. 2018. Major and trace element geochemistry of emerald from several deposits: Implications for genetic models and classification schemes. *Ore Geology Reviews*, **94**, 351–366, https://doi.org/10.1016/j.oregeorev.2018.02.001.

Bendinelli, T., Biggio, L., Nyfeler, D., Ghosh, A., Tollan, P., Kirschmann, M.A. & Fink, O. 2024. GEMTELLIGENCE: Accelerating gemstone classification with deep learning. *Communications Engineering,* **3**(1), article 110, https://doi.org/10.1038/s44172-024-00252-x.

Bindereif, S., Rüll, F., Schwarzinger, S. & Schwarzinger, C. 2020. Chemometric modeling of trace element data for origin determination of demantoid garnets. *Minerals,* **10**(12), article 1046, https://doi.org/10.3390/min10121046.

Bosshart, G. 1991. Emeralds from Colombia (part 2). *Journal of Gemmology*, **22**(7), 409–425, https://doi.org/10.15506/jog.1991.22.7.409.

Cronin, D.P. & Rendle, A.M. 2012. Determining the geographical origins of natural emeralds through nondestructive chemical fingerprinting. *Journal of Gemmology*, **33**(1), 1–13, https://doi.org/10.15506/JoG.2012.33.1.1.

Giuliani, G., Groat, L., Marshall, D., Fallick, A. & Branquet, Y. 2019. Emerald deposits: A review and enhanced classification. *Minerals*, **9**(2), article 105, https://doi.org/10.3390/min9020105.

Groat, L., Giuliani, G., Marshall, D. & Turner, D. 2014. Emerald. *In:* Groat, L.A. (ed) *The Geology of Gem Deposits*, 2nd edn. Mineralogical Association of Canada Short Course Series 44, Québec, Canada, 135–174.

Huong, L.T.-T., Häger, T. & Hofmeister, W. 2010. Confocal micro-Raman spectroscopy: A powerful tool to identify natural and synthetic emeralds. *Gems & Gemology*, **46**(1), 36–41, https://doi.org/10.5741/gems.46.1.36.

Karampelas, S. & Pardieu, V. 2024. Gem Notes: Emerald mining in Musakashi, Zambia. *Journal of Gemmology*, **39**(3), 203–204, https://doi.org/10.15506/JoG.2024.39.3.203.

Karampelas, S., Al-Shaybani, B., Mohamed, F., Sangsawong, S. & Al-Alawi, A. 2019. Emeralds from the most important occurrences: Chemical and spectroscopic data. *Minerals*, **9**(9), article 561, https://doi.org/10.3390/min9090561.

Klemm, L. 2010. *Fieldtrip to Emerald Mines in Zambia, Summer 2010*. Gübelin Gem Lab Ltd, Lucerne, Switzerland, 6 pp., https://tinyurl.com/5xmkrwk9.

Krzemnicki, M.S. 2023. Emeralds from Musakashi (Zambia) and Not from Afghanistan. *Facette Magazine*, No. 28, 42–43, https://www.ssef.ch/wp-content/uploads/2023/05/facette-2023-web.pdf.

Krzemnicki, M.S., Wang, H.A.O. & Büche, S. 2021a. A new type of emerald from Afghanistan's Panjshir Valley. *Journal of Gemmology*, **37**(5), 474–495, https://doi.org/10.15506/JoG.2021.37.5.474.

Krzemnicki, M.S., Wang, H.A.O. & Cartier, L.E. 2021b. Gem Notes: New emeralds from Musakashi, Zambia, appear on the market. *Journal of Gemmology*, **37**(8), 769–771, https://doi.org/10.15506/JoG.2021.37.8.769.

Manyepa, J. & Mutambo, V.P. 2024. Approaches for designing extraction methods for randomly occurring pocket formation of gemstones: A case of Musakashi emerald area, Solwezi, Zambia. *Journal of Mining and Environment*, **12**(3), 605–618, https://doi.org/10.22044/jme.2021.10661.2024.

Ng'uni, B. & Mwamba, K. 2004. *Evaluation of the Potential and Authentication of Emerald Mineralization in North-Western Province, Musakashi Area, Chief Mujimanzovu – Solwezi District*. Draft Geological Report, Geological Survey Department, Lusaka, Zambia, 23 pp.

Pardieu, V., Detroyat, S., Sangsawong, S. & Saeseaw, S. 2015. Tracking emeralds from the Musakashi area of Zambia. *InColor*, No. 29, 18–25.

Saeseaw, S., Pardieu, V. & Sangsawong, S. 2014. Three-phase inclusions in emerald and their impact on origin determination. *Gems & Gemology*, **50**(2), 114–132, https://doi.org/10.5741/gems.50.2.114.

Schmetzer, K. 2014. Letters: Analysis of three-phase inclusions in emerald. *Gems & Gemology*, **50**(4), 316–319.

Schwarz, D. 2015. The geographic origin of emeralds. *InColor*, Special Issue, December, 98–105, http://www.incolormagazine.com/books/grmq/#p=98.

Schwarz D. & Klemm, L. 2012. Chemical signature of emerald. *34th International Geological Congress*, 5–10 August, Brisbane, Australia, abstract 2812.

Schwarz D. & Curti, M. 2020. *Emerald Modern Gemmology*. Bellerophon Gemlab Ltd, Bangkok, Thailand, 481 pp.

SSEF 2021. Press Release: New emeralds from Musakashi in Zambia appear in the market. Swiss Gemmological Institute SSEF, https://www.ssef.ch/new-emeralds-from-musakashi-in-zambia-appear-in-the-market, accessed 15 August 2024.

Taran, M.N. & Rossman, G.R. 2001. Optical spectroscopic study of tuhualite and a re-examination of the beryl, cordierite, and osumilite spectra. *American Mineralogist*, **86**(9), 973–980, https://doi.org/10.2138/am-2001-8-903.

van der Maaten, L. & Hinton, G. 2008. Visualizing data using t-SNE. *Journal of Machine Learning Research*, **9**, 2579–2605, https://www.jmlr.org/papers/volume9/vandermaaten08a/vandermaaten08a.pdf.

Wang, H.A.O. & Krzemnicki, M.S. 2021. Multi-element analysis of minerals using laser ablation inductively coupled plasma time of flight mass spectrometry and geochemical data visualization using t-distributed stochastic neighbor embedding: Case study on emeralds. *Journal of Analytical Atomic Spectrometry*, **36**(3), 518–527, https://doi.org/10.1039/d0ja00484g.

Wang, H.A.O., Krzemnicki, M.S., Chalain, J.-P., Lefèvre, P., Zhou, W. & Cartier, L. 2016. Simultaneous high sensitivity trace-element and isotopic analysis of gemstones using laser ablation inductively coupled plasma time-of-flight mass spectrometry. *Journal of Gemmology*, **35**(3), 212–223, https://doi.org/10.15506/JoG.2016.35.3.212.

Wang, H.A.O., Krzemnicki, M.S., Büche, S., Schmid, R. & Braun, J. 2019. Multi-element analysis of gemstones and its application in geographical origin determination. *36th International Gemmological Conference,* Nantes, France, 28–31 August, 176–178.

Wang, H.A.O., Krzemnicki, M.S., Büche, S., Degen, S., Franz, L. & Schultz-Guttler, R. 2021. Multi-element correlation analysis of Cu-bearing tourmaline using LA-ICP-time of flight-MS. *EUG General Assembly 2021*, online, 19–30 April, abstract EGU21-16170, https://doi.org/10.5194/egusphere-egu21-16170.

Wood, D.L. & Nassau, K. 1968. The characterization of beryl and emerald by visible and infrared absorption spectroscopy. *American Mineralogist,* **53**(5–6), 777–800, http://www.minsocam.org/ammin/AM53/AM53_777.pdf.

Zwaan, J.C., Seifert, A.V., Vrána, S., Laurs, B.M., Anckar, B., Simmons, W.B., Falster, A.U., Lustenhouwer, W.J. *et al*. 2005. Emeralds from the Kafubu area, Zambia. *Gems & Gemology*, **41**(2), 116–148, https://doi.org/10.5741/gems.41.2.116.

The Authors

Dr Michael S. Krzemnicki FGA[1,2,*], Dr Hao A. O. Wang FGA[1], Dr Markus Wälle[1], Pierre Lefèvre[1], Dr Wei Zhou FGA[1] and Dr Laurent E. Cartier FGA[1]

[1] Swiss Gemmological Institute SSEF, Aeschengraben 26, 4051 Basel, Switzerland

[2] Department of Environmental Sciences, University of Basel, Bernoullistrasse 32, 4056 Basel, Switzerland

*Email: michael.krzemnicki@ssef.ch

Acknowledgements

The authors thank the staff of the Swiss Gemmological Institute SSEF, namely Alexander Klumb, Michael Rytz and Chiara Parenzan, and the analytical team consisting of Judith Braun, Gina Brombach, Susanne Büche and Hannah Amsler, for their contributions and analytical work on the investigated emerald samples. Further thanks to Dr Leo Klemm (Lukusuziriver.com, Niederlenz, Switzerland) and A. Jain (Napra Gems B.v.b.a., Antwerp, Belgium) for providing emerald samples from Musakashi for our SSEF research collection.